Cooperative Chemisorption-Induced Physisorption of CO_2 Molecules by Metal–Organic Chains

Min Feng[†,‡] **and Hrvoje Petek**[*,†]

[†]Department of Physics and Astronomy and Pittsburgh Quantum Institute, University of Pittsburgh, Pittsburgh, Pennsylvania 15260, United States and [‡]Institute of Physics, Chinese Academy of Sciences, Beijing 100190, China

Yongliang Shi,[§] **Hao Sun,**[§] **and Jin Zhao**[†,§,∥]

[§]Hefei National Laboratory for Physical Sciences at Microscale and Department of Physics, University of Science and Technology of China, Hefei, Anhui 230026, China and [∥]Synergetic Innovation Center of Quantum Information & Quantum Physics, University of Science and Technology of China, Hefei, Anhui 230026, China

Florencia Calaza,[⊥] **Martin Sterrer,**[*,⊥,#] **and Hans-Joachim Freund**[⊥]

[⊥]Department of Chemical Physics, Fritz-Haber-Institute der Max-Plank-Gesellschaft, Faradayweg 4-6, D-14195 Berlin, Germany and [#]Institute of Physics, University of Graz, Universitätsplatz 5, A-8010 Graz, Austria

ABSTRACT Effective CO_2 capture and reduction can be achieved through a molecular scale understanding of interaction of CO_2 molecules with chemically active sites and the cooperative effects they induce in functional materials. Self-assembled arrays of parallel chains composed of Au adatoms connected by 1,4-phenylene diisocyanide (PDI) linkers decorating Au surfaces exhibit self-catalyzed CO_2 capture leading to large scale surface restructuring at 77 K (*ACS Nano* 2014, *8*, 8644–8652). We explore the cooperative interactions among CO_2 molecules, Au-PDI chains and Au substrates that are responsible for the self-catalyzed capture by low temperature scanning tunneling microscopy (LT-STM), X-ray photoelectron spectroscopy (XPS), infrared reflection absorption spectroscopy (IRAS), temperature-programmed desorption (TPD), and dispersion corrected density functional theory (DFT). Decorating Au surfaces with Au-PDI chains gives the interfacial metal–organic polymer characteristics of both a homogeneous and heterogeneous catalyst. Au-PDI chains activate the normally inert Au surfaces by promoting CO_2 chemisorption at the Au adatom sites even at <20 K. The $CO_2^{\delta-}$ species coordinating Au adatoms in-turn seed physisorption of CO_2 molecules in highly ordered two-dimensional (2D) clusters, which grow with increasing dose to a full monolayer and, surprisingly, can be imaged with molecular resolution on Au crystal terraces. The dispersion interactions with the substrate force the monolayer to assume a rhombic structure similar to a high-pressure CO_2 crystalline solid rather than the cubic dry ice phase. The Au surface supported Au-PDI chains provide a platform for investigating the physical and chemical interactions involved in CO_2 capture and reduction.

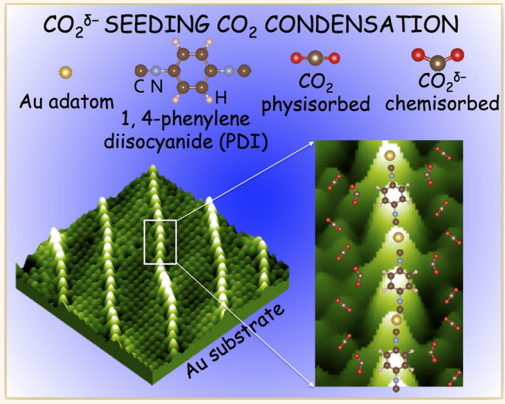

KEYWORDS: CO_2 · $CO_2^{\delta-}$ · CO_2 reduction · CO_2 cluster · chemisorption induced physisorption · metal–organic chains · 1,4-phenylene diisocyanide

The CO_2^- anion radical with a symmetric bent structure is the key precursor in CO_2 reduction in the homogeneous and heterogeneous catalysis.[1−4] A particular challenge in reduction of CO_2 by heterogeneous catalysis is to render metal surfaces sufficiently reactive to form the CO_2^- intermediate, and to promote further reduction to products such as carboxylates, oxalates, or products thereof,[5−19] avoiding the poisoning carbonate species.[3,19−31] Although chemisorption occurs on some transition metals, activated formation of a partially reduced $CO_2^{\delta-}$ species has only been imaged at the single-molecule level on the defect-free Ni(110) surface.[32] By contrast, clean and defect-free noble metal surfaces are unreactive with respect to CO_2 chemisorption. Chemisorption of CO_2 can be promoted, however, by defects such as steps and kinks,

* Address correspondence to petek@pitt.edu, martin.sterrer@uni-graz.at.

Received for review August 18, 2015 and accepted November 7, 2015.

Published online November 07, 2015
10.1021/acsnano.5b05222

or by predecorating otherwise inert surfaces with catalytically active atoms or molecules.[1] Here we report on a novel method for chemically activating single crystal Au surfaces with respect to the $CO_2^{\delta-}$ formation by decorating them with an interfacial metal organic polymer consisting of highly ordered 1D chains, which create Au adatom active sites. The chemisorption of CO_2 ligands at such sites in-turn triggers CO_2 physisorption in highly ordered 2D van der Waals monolayer.

In a previous study, we have shown that CO_2 adsorption onto Au(100) and Au(111) surfaces decorated with 1D metal−organic chains (MOCs) composed of alternating units of 1,4-phenylene diisocyanide molecules and Au adatoms (Au-PDI) triggers self-catalyzed CO_2 adsorption involving pronounced nanometer scale MOC's motion. Individually the PDI molecules and Au surfaces are both catalytically inert with respect to CO_2 chemisorption, but as a metal−organic interfacial polymer decorating Au surfaces they become catalytically active. By molecule resolved LT-STM imaging we show that the trigger for the catalytic response is CO_2 chemisorption. Single molecule resolved imaging shows that the chemisorption of CO_2 occurs at <20 K with up to two $CO_2^{\delta-}$ species coordinating each Au adatom, one on each side, within the Au-PDI chains. The $CO_2^{\delta-}$ species in-turn seed further condensation of highly ordered physisorbed CO_2 clusters, which grow with increasing coverage into ordered molecular monolayer films that otherwise do not condense on Au surfaces. The seeding effect of $CO_2^{\delta-}$ enables unprecedented imaging of surface-supported 1D and 2D $CO_2^{\delta-}\cdot(CO_2)_n$ clusters as large as complete monolayer domains with single molecule resolution. The interaction of thus seeded CO_2 films with the Au metal substrates causes the CO_2 monolayer to form a highly ordered structure reminiscent of the high-pressure CO_2 face-centered rhombic phase,[33,34] rather than the common cubic "dry ice" phase. DFT calculations show that van der Waals interactions with the substrate favor this unexpected phase. Temperature dependent XPS and IRAS, as well as TPD measurements confirm the presence of the physisorbed and chemisorbed CO_2 phases and give their desorption temperatures of 115 and 150 K, respectively. The ability to catalyze, resolve, and spectroscopically characterize the chemical and physical properties of $CO_2^{\delta-}\cdot(CO_2)_n$ clusters interacting with metal−supported metal−organic constructs at the molecular level opens the way to study CO_2 reduction in the presence of electron, photon, and chemical reagents.

CO_2 Adsorption Structures. Upon vapor phase deposition at 300 K, PDI molecules self-assemble into highly ordered Au-PDI chains on the Au(100) and Au(111) surfaces.[35−39] The interaction among the Au-PDI chains is repulsive forcing them to spread out to achieve a uniform, coverage-dependent spacing at 77 K. We have reported that upon CO_2 adsorption the chain interactions become attractive causing them to coalesce and capture CO_2 molecules that become intercalated between them.[39] Figure 3 of ref 39 illustrates the lateral gathering movement of the chains, whereby CO_2 molecules became captured in one-molecule-wide ranks between the adjacent chains. On isolated chains or at chain bundle edges the motion of peripheral CO_2 molecules is unconstrained; this motion relative to the chains is captured in STM images as halo structures, which emanate from Au adatoms and encircle the PDI molecules. Within these halo structures the closest approach of CO_2 molecules occurs at Au adatoms, which suggests that the strongest CO_2 molecule-MOC interaction occurs at these sites.[39] These observations suggested that CO_2 chemisorption occurs at the Au adatom sites and the concomitant charge redistribution induces the chain coalescence.[39]

RESULTS

CO_2 Monomer Adsorption on Au-PDI/Au(100). To gain further information on the interaction of CO_2 molecules with Au-PDI chains through STM imaging, in this study we perform LT-STM experiments at 4.5 K to freeze substantially their translational motion. As a reference for the nature of interactions of CO_2 molecules on the *undecorated*, *i.e.*, bare Au(100)-(5 × 20) reconstructed surface, in Figure 1a we first show images taken at 4.5 K after dosing of CO_2 at 20 K. CO_2 molecules at submonolayer coverage on unmodified Au surface cluster through quadrupole−quadrupole interactions into physisorbed chemically inert rafts. These structures appear as bright, unresolved contrast with extensive streaking indicative of tip-induced molecular displacement.[3,40−42] Such CO_2 clusters interact with Au surfaces through a weaker van der Waals interaction than within the clusters; consequently, the CO_2 aggregates are mobile and/or easily disturbed by the STM tip, preventing molecule-resolved imaging of stable structures even at 4.5 K.

By contrast to the bare surface, decorating the Au(100) surface with the Au-PDI chains causes CO_2 molecules to adsorb in stable structures that preferentially coordinate the Au adatom sites; this attraction enables imaging of the interaction of single CO_2 molecules with Au-PDI chains at 4.5 K (Figure 1b,c). Such preferred interaction of CO_2 molecules with Au adatoms was already presaged by the halo structures at 77 K.[39] Although it is difficult to diagnose charge transfer only by STM imaging, we claim that CO_2 is chemisorbed at the Au adatoms sites as $CO_2^{\delta-}$, and we will show by XPS, IRAS, and TPD that such species exists when Au-PDI chain decorated Au surfaces are exposed to CO_2. Based on the STM imaging we can conclude that the strongest interaction experienced by CO_2 molecules occurs at the Au adatoms sites within Au-PDI chains.

The $CO_2^{\delta-}$ species in Figure 1b,c are imaged at 4.5 K as a two-lobed "rabbit ears" structures on one and

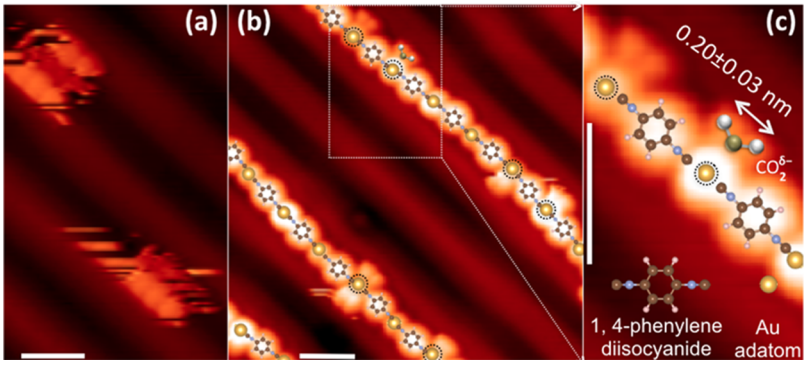

Figure 1. (a) STM image acquired at 4.5 K after dosing CO_2 molecules onto the clean Au(100) surface. The periodic background contrast is from the 5 × 20 reconstruction. The ragged, bright contrast is from CO_2 islands, which are highly mobile and perturbed by the STM tip even at 4.5 K. (b) STM image at 4.5 K of the Au-PDI chain modified Au(100) surface after submonolayer of CO_2 is dosed at 20 K. The image shows occasional CO_2 monomers adsorbed alongside the Au adatoms. Black dashed circles indicate Au adatoms hosting the chemisorbed $CO_2^{\delta-}$. (c) The magnified image of the rectangular region in (b) showing the chemisorbed $CO_2^{\delta-}$. The Au adatoms, PDI molecules, and one $CO_2^{\delta-}$ are marked with model structures as in (b). The molecular structure shown for one of the two $CO_2^{\delta-}$ in the image is based on the simulated STM imaging in the Supporting Information Figure S1. The white bars indicate 1 nm scale.

occasionally both sides of Au adatoms. The high-resolution image in Figure 1c resolves the center-to-center distance between the lobes of 0.20 ± 0.03 nm. Considering that 0.232 nm separates the O atoms of a linear CO_2 molecule,[43] the rabbit ear structure is consistent with resolving them within a single molecule. The structure in Figure 1c that is superimposed above one of the $CO_2^{\delta-}$ images in Figure 1c is based on the simulated STM imaging in the Figure S1 (Supporting Information). The rabbit ear structures uniquely appear at the Au adatom sites, and cannot be assigned to CO_2 van der Waals dimers. Furthermore, because single-lobe images cannot be found for *single* CO_2 molecules at Au adatom sites and STM manipulation experiments (see below) cannot create them, we conclude that the rabbit ears structures are the characteristic images of CO_2 monomers chemisorbed at Au adatom sites. The actual structure of the chemisorbed CO_2 molecules is uncertain, however, because the carbon atom is not resolved. Moreover, it is also possible that STM is imaging single CO_2 molecules interchanging between two equivalent sites through thermal or STM tip-induced stimulation at 4.5 K.

CO_2 Cluster Condensation on Au-PDI/Au(100). The chemisorbed Au-$CO_2^{\delta-}$ species seed further CO_2 molecule condensation and anchor thus formed $CO_2^{\delta-}\cdot(CO_2)_n$ clusters, as seen in Figure 2. Note that stable CO_2 clusters form only at the seeding sites, which is consistent with the interaction between the anionic $CO_2^{\delta-}$ and the quadrupolar neutral CO_2 molecules. No CO_2 molecule appears next to a PDI site without simultaneously interacting with a $CO_2^{\delta-}$ anchor molecule. When physisorbed CO_2 molecules interact with $CO_2^{\delta-}$, the two-lobed image of the anchoring molecule disappears. Instead, dimers and larger assemblies are characterized by centers of bright contrast having typical distances of 0.40 ± 0.03 nm (Figure 2) that is typical for CO_2 molecules assembled through the quadrupole−quadrupole interactions.[43]

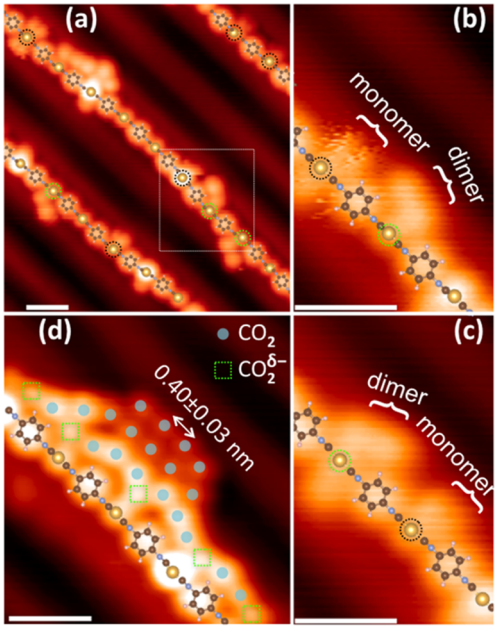

Figure 2. (a) STM image of CO_2 monomers, dimers and larger clusters on Au(100) surface at 4.5 K. The black and green dashed circles around the golden spheres mark the Au adatom sites with CO_2 monomers and dimers, respectively. (b) A typical structure motif with a CO_2 monomer and dimer on the adjacent Au adatom sites also seen in (a) within the white rectangle. (c) STM image of the same region as in (b) after STM tip manipulation of the physisorbed CO_2 between the adjacent $CO_2^{\delta-}$ anchoring species. The manipulation interchanges reversibly the two-lobed structure of a $CO_2^{\delta-}$ monomer and the ball structure of $CO_2^{\delta-}$ in the dimer. Theoretical simulations in Figure S1 qualitatively reproduce the monomer and dimer images. (d) STM image showing the incipient formation of an ordered 2D CO_2 island on one side of a 1D CO_2 cluster. Physisorbed CO_2 molecules are marked by blue dots. The indicated separation between centers of bright contrast is typical of CO_2 distances in van der Waals clusters. White bars mark 1 nm scale.

To confirm that the anchoring molecule in dimers is the same species as a $CO_2^{\delta-}$ monomer with the two-lobed structure we performed molecular manipulation

experiments using the STM tip. In Figure 2b,c, we drag one CO_2 molecule from a dimer to a solitary neighboring $CO_2^{\delta-}$ with the rabbit ear structure on the same Au-PDI chain. After the manipulation, the released $CO_2^{\delta-}$ recovers its two-lobed appearance, and simultaneously, the newly formed dimer losing its original two-lobed structure takes on the characteristic image of the original dimer. The change of the chemisorbed $CO_2^{\delta-}$ image between the monomer and dimer may indicate that $CO_2^{\delta-}$ reorientation upon forming the dimer, or else the rabbit ear structure represents fluctuation of $CO_2^{\delta-}$ between two equivalent sites at 4.5 K, one of which is hindered by the dimer formation. The former interpretation is consistent with the calculated structure of $CO_2^{\delta-}\cdot CO_2$ and its STM imaging in the Supporting Information Figure S1. The manipulation of the physisorbed CO_2 molecule between the adjacent seeding sites can be reversed. These manipulation experiments confirm our assignment of the CO_2 monomer and dimer structures.

Our experiments further reveal that $CO_2^{\delta-}$ species seed and anchor the nucleation and growth of 1D and 2D CO_2 molecular clusters. Figure 2d shows a 1D CO_2 cluster formed next to an MOC chain. For each Au-PDI unit there is one $CO_2^{\delta-}$ seed interacting with an Au adatom and 2−3 associated physisorbed CO_2 molecules solvating the PDI ligand. Figure 2d also shows further emergence of a CO_2 island from the 1D CO_2 chain with consistent intermolecular distances of ~0.4 nm. As no such island can be resolved by STM on the bare Au(100) surface under the same experimental conditions, we claim that exclusively physical interaction among CO_2 molecules and with the substrate cannot explain the molecule resolved imaging of stable CO_2 islands. The formation and imaging of stable clusters is consistent with chemisorption of CO_2 at the Au adatom sites to form $CO_2^{\delta-}$, which further seeds and stabilizes the condensation of neutral CO_2 molecules as in the case of gas-phase CO_2 ionic clusters.[44] The difference between the ionic and neutral CO_2 clusters reflects the large quadrupole moment and polarizability of CO_2 molecules, which enable them to screen and solvate doped charges.[39] Complementary LT-STM measurements on MOC decorated Au(111) surface in the next section confirm that the PDI-Au chains confer the ability to chemisorb and physisorb CO_2 molecules independent of the particular properties, *e.g.*, the crystalline order or work function of the Au substrate.

From CO_2 Clusters to Monolayer on Au-PDI/Au(111) Surface. Here we establish by STM imaging that Au-PDI chain covered Au(111) and Au(100) surfaces have the same specific adsorption sites for CO_2 molecules at 4.5 K. Furthermore, we extend the cluster growth to full CO_2 monolayers on the Au-PDI/Au(111) surface.

Figure 3a,b shows typical CO_2 monomers, dimers and islands formed alongside of Au-PDI chains on the Au(111) surface. As on the Au-PDI/Au(100) surface, the CO_2 monomers and dimers on the Au-PDI/Au(111) surface adopt the same two-lobe and ball structures at low coverages (Figure 3a). Larger CO_2 clusters, as shown in Figure 3b, have two characteristic structures, the compact rhombic monolayer and the hexagonal missing-molecule defect. The clusters grow to a monolayer, forming crystalline stripes that fill the interstitial space between the Au-PDI chains. Figure 3b shows a large area view of the monolayer film where the bright contrast represents the Au-PDI chains, which are aligned along three high symmetry directions of the surface, and the darker contrast corresponds to individual CO_2 molecules forming the monolayer in the space between the MOC chains; the contrast is modulated by the underlying herringbone reconstruction of the substrate. In Figure 3d,e consecutive images are taken over the same area of CO_2 monolayer stripes to show that the hexagonal defects move through the layer even at 4.5 K; this occurs most likely by translation of single molecules from the compact rhombic domains to the missing molecule defects that correspond to the hexagonal lattice. The facile mobility of the CO_2 molecules within a monolayer other than at the seeding sites is consistent with their physisorption state.

Although the structure of the monolayer CO_2 stripes is established by physical interactions, it is clear from the structure of CO_2 clusters and the magnified image of the monolayer in Figure 3f that the growth is promoted by chemisorption of two CO_2 molecules, one on each side of the Au adatoms. Moreover, the dark contrast between CO_2 and PDI shows that the interaction between CO_2 and phenyl group of PDI is primarily repulsive.[45] The attachment of single CO_2 molecules to the Au sites and their absence around the PDI sites establish that the $CO_2^{\delta-}$ is the seed and anchor for the nucleation and condensation of the monolayer stripes.

Finally, we test the length scale over which the CO_2 monolayer crystalline structures can form as the MOC chain separation is increased. In Figure 4 we show a monolayer CO_2 film with sparse Au-PDI chains where the interchain distance ranges from 8 to 22 nm. We see that even for such sparse MOC chain density, the $CO_2^{\delta-}$ chemisorption at the Au seeding sites enables crystallization of a full monolayer with high local crystalline order. The predominant rhombic structure with several rotational domains is interspersed with stripes of hexagonal defect structures, forming a kagome lattice. Thus, the presence of a small density of chemisorption sites on MOC chains is able to seed the 2D CO_2 crystalline growth over the entire atomically flat Au(111) terraces.

Upon formation of a full CO_2 monolayer in Figures 3c and 4 we conclude that (i) CO_2 molecules adopt a highly crystalline order at 4.5 K on Au-PDI decorated gold surfaces, enabling the molecule resolved imaging of CO_2 to be performed from single molecules up to the full monolayer; (ii) the preferred

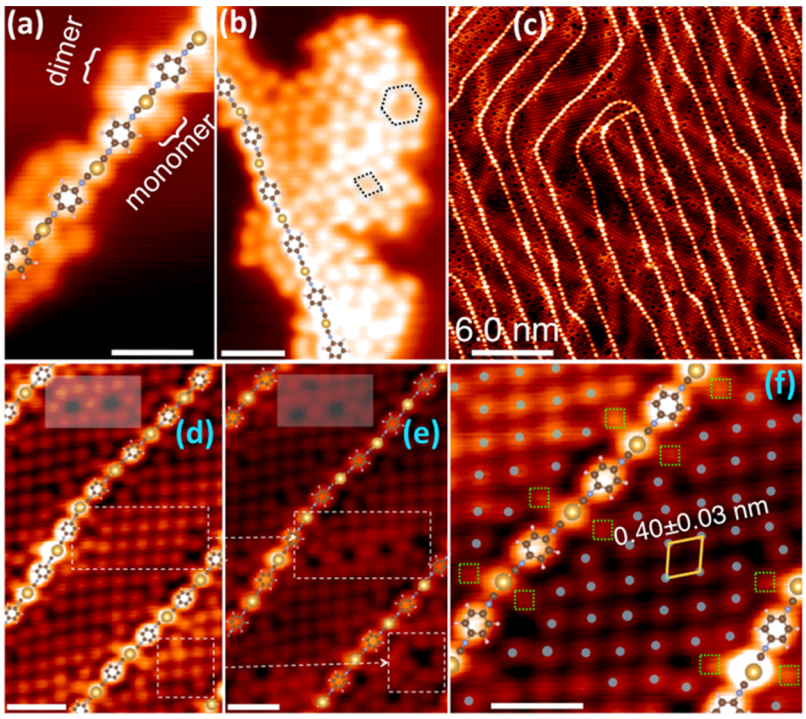

Figure 3. STM image obtained at 4.5 K (a) showing CO_2 monomers, dimers and longer assembles interacting with a Au-PDI chain on the Au(111) surface. CO_2 monomers and dimers have the two-lobed and symmetric ball structures as on the Au(100) surface. (b) STM image of a 2D CO_2 island that is anchored by an Au-PDI chain. Typical rhombic and hexagonal structures within CO_2 islands are indicated. (c) A wide area single molecule-resolved STM image of a full CO_2 monolayer with the predominant rhombic structure that includes hexagonal defects. (d) and (e) Sequential STM images of the same region showing defect motion in the condensed CO_2 monolayer. The two translucent rectangles serve as position markers. The two dashed rectangles indicate the hexagonal defect structures, which appear in the initial compact CO_2 rhombic structure. These changes indicate that CO_2 molecules are mobile on the surface even at 4.5 K. (f) The magnified image shows the rhombic unit cell with dimensions of 0.40 ± 0.03 nm that dominates the CO_2 monolayer structure. The green squares mark CO_2 molecules chemisorbed at the Au sites, and the blue dots the physisorbed CO_2 molecules within the monolayer. White bars indicate 1 nm scale unless indicated otherwise.

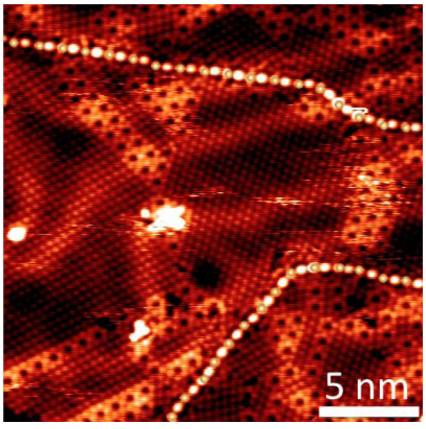

Figure 4. An STM image with sparse Au-PDI chains on Au(111) surface showing that ordered monolayer CO_2 domains can span >20 nm terrace widths. Hexagonal defect domains with a kagome tiling penetrate the rhombic structures with several rotational domains. The Au(111) substrate reconstruction modulates the CO_2 contrast. The Au adatoms within the chains are marked with golden spheres.

structure within a monolayer is the rhombic one with a unit cell dimension of 0.40 ± 0.03 nm and coordination shell of six nearest neighbor molecules; and (iii) the kagome structures exist as less dense domains within the rhombic structure before the full monolayer coverage is reached.

CO_2 Monolayer Structure. Next we consider the physical origin of the rhombic structure of the CO_2 monolayers on both the Au-PDI decorated Au(100) and Au(111) surfaces (Figures 2-4) based on dispersion corrected DFT-D calculations. At the atmospheric pressure crystalline CO_2 molecular solid, *i.e.*, "dry ice", has a cubic structure where CO_2 molecules tilt by 35° with respect to the crystalline planes. CO_2 undergoes a phase transition at 13 GPa from the cubic to an orthorhombic structure with reduced tilting angle of the CO_2 molecules.[33,34] The similarity between the structure of a CO_2 monolayer on Au surfaces and CO_2 solid under high pressure suggests physisorbed molecules experience similar molecular reorientation.

To confirm that a compression is taking place in the first CO_2 monolayer as in the high pressure CO_2 phase, we calculate the monolayer structure and stability using the DFT-D method to incorporate the van der Waals interactions among CO_2 molecules and with the Au(111) surface.[46] The details of the calculations are presented in the Supporting Information, and here we present only the main results. The calculations are performed on $2 \times \sqrt{3}$ and $7 \times \sqrt{3}$ surface unit cells to

model the cubic and rhombic structures, corresponding to the low and high pressure phases of dry ice. The rhombic structure corresponds best to the experimental intermolecular distances and CO_2 film alignment with respect to the Au(111) substrate, whereas the cubic structure is not found in the STM imaging of a CO_2 monolayer, but is considered here as a representation of the dry ice phase.[33,34]

In agreement with experiment, by including the Au(111) surface, the rhombic structure is calculated to be more stable by 82 meV. In cubic structure, CO_2 molecules tilt, forming an angle of 30° with respect to the surface, whereas in the rhombic structure, they are more parallel with an angle of 8°. Tilting of the CO_2 molecules to a more parallel alignment with respect to the surface plane increases the van der Waals interactions with the substrate, and therefore favors the rhombic phase. This additional interaction with the Au surfaces compensates for the increased intermolecular repulsion that exists in the high-pressure rhombic phase of CO_2.

XPS, IRAS, and TPD Probes of CO_2 Adsorption State. The LT-STM imaging shows manifestations of the dominant interactions among CO_2, Au-PDI chains, and Au surfaces, but the charge transfer to CO_2 molecules can only be inferred indirectly. Surface integrated XPS and IRAS measurements, however, can identify the charge state of the adsorbed species. Our goal is to correlate the LT-STM with XPS and IRAS measurements, but because of experimental constraints, the XPS and IRAS cannot be performed at comparably low temperatures. The lowest sample temperature attained in the spectroscopic studies is ~100 K, where, according to our previous investigations, CO_2 adsorption induces Au-PDI chain coalescence and interstitial CO_2 trapping.[39] To distinguish between different states of adsorbed CO_2, we prepare PDI-Au(111) samples with two different PDI coverages: A high-coverage sample corresponding to full monolayer of PDI and a chain separation of 1.4 nm (PDI_H),[39] and a low coverage sample of about half-monolayer and a chain separation of 2.8 nm (PDI_L). Coverage is estimated based on work function shifts upon PDI adsorption,[38] which are typically −1.0 and −0.7 eV for the high- and low-coverage PDI-Au(111) samples, respectively. The −1.0 eV shift corresponds to the maximum MOC coverage attained in our experiments.[39] From the analysis of XPS peak intensities the estimated PDI coverage ratio of PDI_L/PDI_H is Θ_L/Θ_H = 0.5−0.6 (Θ represents the coverage of Au-PDI chains on the surface). While CO_2 adsorbed at peripheral sites of the Au-PDI chains or trapped between Au-PDI chains are present on both samples, we expect physisorbed CO_2 domains to form more abundantly on the PDI_L.

First, we note that CO_2 dosed onto clean Au(111) at 100 K followed by pumping at this temperature does not give a detectable photoemission signal from

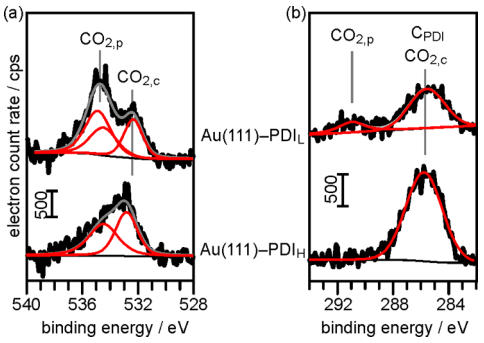

Figure 5. O 1*s* (a) and C 1*s* (b) X-ray photoemission spectra for a saturation coverage of CO_2 at 100 K on Au(111)-PDI_L (top) and Au(111)-PDI_H (bottom). Lines marked $CO_{2,p}$ and $CO_{2,c}$ denote the O 1*s* and C 1*s* binding energies of physisorbed and chemisorbed CO_2 species, respectively. The spectral fitting is explained in the text. Thick black lines: raw spectra; red lines: individual signal contributions obtained from spectral fitting; gray lines: fit sum; thin black lines: background.

adsorbed species. This is consistent with conclusions from the LT-STM experiments that the CO_2 physisorption is enhanced to Au-PDI chain decorated Au surfaces. Therefore, any photoemission peaks from CO_2 on PDI covered Au surfaces have to be a consequence of direct or catalyzed interactions between CO_2 and Au-PDI chains.

Figure 5a,b shows O 1*s* and C 1*s* XP spectra of the two samples after saturating the surface with CO_2 at 100 K. For the low-coverage sample two well-separated O 1*s* peaks appear at binding energies (BEs) of 532.3 and 534.7 eV, respectively. The corresponding C 1*s* region is dominated by the contribution of PDI centered around 285 eV,[47] which is accompanied by a small peak at 291.2 eV. By comparison with previous XPS work on CO_2 adsorption on clean and modified metal surfaces, the high BE XP peaks can readily be assigned to physisorbed CO_2 (534.7 eV for O 1*s* and 291 eV for C 1*s*), whereas the BE of the second O 1*s* signal (532.3 eV) is compatible with $CO_2^{\delta-}$.[48−51] Its corresponding C 1*s* emission is expected at 288−289 eV, however, this region is obscured by the major C 1*s* signal from adsorbed PDI molecules. Although the O 1*s* contribution of physisorbed CO_2 could be fitted with a single, broad peak, we have separated it into two contributions, a choice that is motivated by the TPD and IRAS results reported below. The O 1*s* region of the high-coverage sample is dominated by the signal from $CO_2^{\delta-}$ at 532.3 eV. The spectrum is asymmetric and to obtain a proper fit requires the inclusion of a second, higher BE contribution, pointing to the presence of some additional CO_2 in a different, physisorbed bonding state. Most notably, a large contribution of physisorbed CO_2 with a BE of 534.7 eV and its corresponding C 1*s* signal at 291 eV as observed for the PDI_L sample is not present or maybe not be resolvable on PDI_H. Therefore, the XPS data confirm the existence of at least two chemically distinct CO_2 species on the

PDI-covered Au(111) surfaces, with one of the components present on both PDI_L and PDI_H being in a chemisorbed anionic state, and the other one, which is more abundant on PDI_L, being physisorbed.

The thermal stability of CO_2 on PDI-covered Au(111) is first investigated by TPD (Figure 6a). The bottom CO_2 TPD trace (dotted line) in Figure 6a shows CO_2 desorption from clean Au(111) after exposure to CO_2 at 100 K. Since no surface species can be detected for this preparation with spectroscopic methods (XPS and IRAS), the CO_2 signal is attributed to its desorption from the sample holder. CO_2 trapped on Au(111)-PDI_H gives rise to a broad desorption signal peaking at 125 K and extending up to ~150 K. In addition, the Au(111)-PDI_L sample exhibits a sharp low-temperature CO_2 desorption at 115 K (α). Taking the XPS and TPD results together, it is tempting to assign the latter desorption signal to physisorbed CO_2 and the broader one at 125 K to chemisorbed $CO_2^{\delta-}$. That this assignment needs further refinement will become clear after consideration of the corresponding IRAS results, which are discussed next.

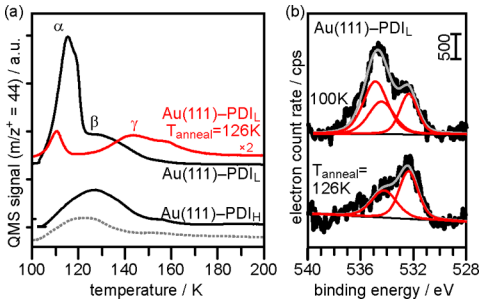

Figure 6. (a) CO_2-TPD spectra taken after CO_2 adsorption on Au(111) at 100 K (dotted line); the observed CO_2 signal is mainly due to CO_2 desorption from the sample holder. Au(111)-PDI_H and Au(111)-PDI_L (black lines) designate CO_2 TPD spectra of Au-PDI chain covered surfaces. The red line shows the CO_2-TPD taken from Au(111)-PDI_L after a cycle of preheating to 126 K and recooling to 100 K. (b) O 1*s* XP spectrum of Au(111)-PDI_L taken after adsorption of CO_2 at 100 K (top), and after a subsequent cycle of heating to 126 K and recooling to 100 K (bottom). Thick black lines: raw spectra; red lines: individual signal contributions obtained from spectral fitting; gray lines: fit sum; thin black lines: background.

To obtain further insight into the adsorption and bonding of CO_2 on the Au(111)-PDI surfaces, the chemical nature of adsorbed species as well as their thermal evolution is probed by IRAS (Figure 7). Before exposure to CO_2, the IRA spectra are dominated by the NC vibrations of adsorbed PDI,[36,48−54] giving rise to bands at 2141 and 2164 cm^{-1} for the high- and low-coverage samples, respectively (top spectra in Figure 7a,b). The coverage-dependent shift concurs with results of previous IRAS studies.[36] The spectra undergo significant changes upon adsorption of CO_2 (blue traces in Figure 7a,b). As will be discussed in more detail below, CO_2 adsorption/desorption induces shifts of the NC vibrations, which appear in Figure 7 as positive and negative peaks according to the choice of the reference spectra for the background subtraction (see Figure 7 caption for details).

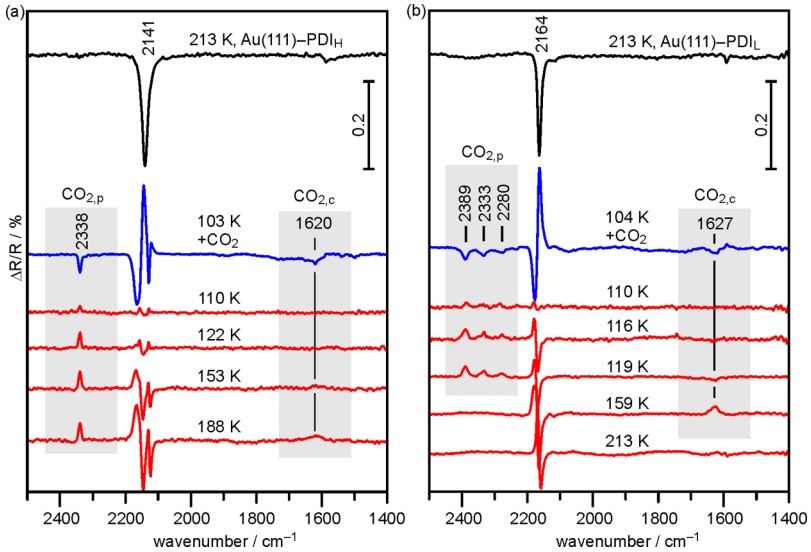

Figure 7. IRA spectra of (a) Au(111)-PDI_H and (b) Au(111)-PDI_L at 213 K without adsorbed CO_2 (black), after saturating the surface with CO_2 at 103 K (blue), and after subsequent heating to the indicated temperatures (red). For the IRAS measurement, a reference spectrum of a clean Au(111) surface at room temperature is recorded first. Then the sample is exposed to PDI and subsequently cooled to 213 K. The resulting IRA spectrum (black) shows the NC vibration as main feature. This spectrum serves as reference for the following ones (blue), which are recorded while cooling the sample with the CO_2 background pressure of 5×10^{-8} mbar (adsorbing species give rise to negative peaks; the presence of both negative and positive peaks in the NC stretching region around 2150 cm^{-1} is caused by frequency shifts of the NC vibration). After reaching the lowest temperature, CO_2 is evacuated from the chamber and a spectrum is recorded. This spectrum then serves as reference for the later ones recorded during the warming phase (red) where desorbing species appear as positive peaks. As the sample is warmed, first the physisorbed ($CO_{2,p}$) and then the chemisorbed CO_2 molecules ($CO_{2,c}$) desorb from the surface.

We will focus now on IRAS signals that can be attributed to adsorbed CO_2. For both, Au(111)-PDI_H (Figure 7a) and Au(111)-PDI_L (Figure 7b), new bands appear at around 2340 and 1620 cm^{-1}, respectively, after adsorption of CO_2. For Au(111)-PDI_H, the single band observed at 2338 cm^{-1}, which is slightly red-shifted from the antisymmetric stretch vibration (ν_3) of gas-phase CO_2 (2349 cm^{-1}), can be attributed to physisorbed CO_2, the shift arising from weak interaction with the substrate. The other band at 1620 cm^{-1} is assigned to the antisymmetric stretch vibration of the bent $CO_2^{\delta-}$ anion, in agreement with previous studies of CO_2^- adsorbed on metals[1,10,55,56] or isolated in rare-gas matrix.[57−59] We note that carbonate would also give an IR signal at around 1600 cm^{-1}. We consider this assignment to be unlikely, because carbonates are thermally much more stable than the species observed here (see below), and a source of oxygen atoms necessary for their formation is lacking.

On the basis of the established correlation between the $CO_2^{\delta-}$ ν_3 frequency and the degree of charge transfer, the observed peak at 1620 cm^{-1} is consistent with a transfer of significant charge approaching 1 e^- to the CO_2.[1,58,60,61] A similar band at 1627 cm^{-1} due to $CO_2^{\delta-}$ is found for Au(111)-PDI_L (Figure 6b, blue trace). In the ν_3 region of the physisorbed CO_2, however, instead of a single band, at least three bands appear: one at 2333 cm^{-1}, slightly red-shifted from the corresponding signal on Au(111)-PDI_H, and two additional ones at 2389 and 2280 cm^{-1}. As expected, the physisorbed CO_2 is more weakly bound and has desorbed from both surfaces (PDI_H and PDI_L) upon heating to ~120 K (red spectra in Figure 7a,b; due to the choice of the reference spectrum, the desorbing species appear as positive signals), but the more strongly bound chemisorbed $CO_2^{\delta-}$ is stable up to ~150 K in agreement with the TPD results presented above.

The interaction of CO_2 with Au-PDI chains on the Au(111) surfaces is also manifested in distinct frequency shifts of the NC stretch vibration shown in Figure 8a for Au(111)-PDI_L. The NC vibration shifts from 2166 to 2176 cm^{-1} upon cooling in CO_2 atmosphere from 159 to 104 K. Upon subsequent sample warming, the CO_2 adsorption remains unaffected up to 110 K where, according to Figure 7, no significant desorption occurs. Further warming to 116 and 119 K, however, removes all the physisorbed CO_2 from the surface, leading to a partial return of the NC frequency to its noninteracting value. A clear high-frequency shoulder centered at about 2180 cm^{-1}, however, remains in this temperature range, and disappears only after further heating to 159 K (Figure 7a) when the chemisorbed $CO_2^{\delta-}$ has desorbed (Figure 6b). This shoulder therefore can be directly associated with the chemisorbed $CO_2^{\delta-}$ where the blue-shift arises from charge-transfer from the $2\pi^*$ state of NC through the Au adatom to $CO_2^{\delta-}$.

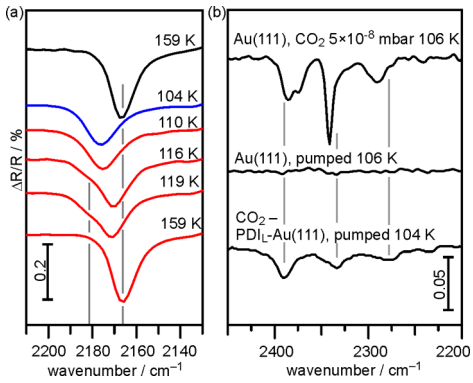

Figure 8. (a) IRAS spectral detail of the NC vibration of PDI molecules on Au(111)-PDI_L at 159 K (black), after saturation with CO_2 at 104 K (blue) and subsequent heating to 110, 116, 119, and 159 K (red). The vertical lines in Figure 8a mark the spectral position of the unperturbed NC vibration at 2166 cm^{-1} and of the NC vibration affected by adsorbed $CO_2^{\delta-}$ at 2182 cm^{-1} (see text for details). (b) CO_2—IRAS spectra taken of Au(111) exposed continuously to 5 × 10^{-8} mbar CO_2 at 106 K (top) and after subsequent evacuation at 106 K (middle). For comparison, the bottom spectrum shows the IRA spectrum of stable CO_2 species on Au(111)-PDI_L at 104 K.

According to the distinct difference in thermal stability of physisorbed CO_2 and $CO_2^{\delta-}$, a spectral isolation of the individual components by controlled heating should be similarly possible in TPD and XPS as it is in IRAS. Figure 6b displays XPS spectra taken from Au(111)-PDI_L following CO_2 adsorption at 100 K (upper spectrum) and subsequent heating to 126 K (lower spectrum), confirming that physisorbed CO_2 has to a large extent been selectively removed from the surface by the thermal treatment (the high BE shoulder present in the XP spectrum of the heated sample can most likely be attributed to CO_2 species readsorbed after recooling to 100 K). The remaining chemisorbed $CO_2^{\delta-}$ gives rise to a CO_2 desorption signal peaking at 145 K (red trace in Figure 6a), suggesting that the broad desorption feature observed in the TPD spectra contains partly overlapping desorption states of physisorbed (β) and chemisorbed (γ) CO_2.

The combination of XPS, IRAS, and TPD results thus provides a very consistent interpretation of the spectroscopic observations in terms of the presence of various CO_2 species adsorbed on the Au(111)-PDI surfaces (Table 1): The most strongly bound CO_2 species is chemisorbed $CO_2^{\delta-}$. Its assignment is supported by the signature O 1*s* BE (~532 eV), the vibrational frequency (1620 cm^{-1}) and the fact that it is the most strongly bound CO_2 species (TPD peak γ). According to the LT-STM imaging, this species is adsorbed at the Au adatom sites of Au-PDI chains and acts as the seed for further CO_2 adsorption. The second CO_2 species, which is present on both surfaces, is physisorbed CO_2 exhibiting an O 1*s* BE of 534.5 eV and a vibrational frequency slightly red-shifted from ν_3 of gas-phase CO_2 (species β in TPD). This species is attributed to CO_2 molecules,

TABLE 1. Summary of O 1*s* and C 1*s* Binding Energies, Desorption Temperature, and CO_2 Vibrational Frequencies of the Different CO_2 Species Adsorbed on Au(111)-PDI_H and Au(111)-PDI_L[a]

CO_2 species	O 1*s*/eV	C 1*s*/eV	T_{des}/K	$\nu(CO_2)$/cm^{-1}
Chemisorbed CO_2, $CO_2^{\delta-}$				
Au(111)-PDI_H	532.8	n.o.	145 (γ)	1620
Au(111)-PDI_L	532.3	n.o.		1627
Physisorbed CO_2, trapped				
Au(111)-PDI_H	534.5	n.o.		2338
Au(111)-PDI_L	534.5	n.o.	125 (β)	2333
Physisorbed CO_2, 2D islands				
Au(111)-PDI_H	—	—	—	—
Au(111)-PDI_L	534.8	291.2	115 (α)	2389, 2280

[a] n.o. indicates "not observed".

which get trapped between PDI chains upon CO_2 adsorption-induced chain coalescence, as observed in our previous STM study (Figure 3 of ref 39.). Finally, there is a third CO_2 species, which is only present on Au(111)-PDI_L. Its O 1*s* BE is typical of physisorbed CO_2. Unlike the other physisorbed species present on the surfaces, however, this species gives rise to a relatively sharp desorption peak at low temperature (peak α), and to two vibrations that are shifted $\sim$50 cm^{-1} to both sides of the ν_3 of CO_2. Because this species does not appear on the densely packed Au(111)-PDI_H sample we assign the corresponding adsorption state to 2D CO_2 monolayer stabilized on the exposed Au(111) areas of Au(111)-PDI_L by the chemisorbed $CO_2^{\delta-}$.

Whereas the assignment of the first two CO_2 species is relatively straightforward, we consider the interpretation of the third species as arising from 2D CO_2 monolayer to be speculative, because it is mainly motivated by the STM observations made at 4.5 K. Such species could exist on Au-PDI decorated surfaces at 77 K, but in a motional state that cannot be imaged by LT-STM. To provide more solid basis for the assignment, in Figure 8b we compare IRA spectra following CO_2 adsorption at $\sim$100 K on the clean Au(111) and Au(111)-PDI_L surfaces. As already noted, interaction between CO_2 and clean Au(111) is weak and does not yield any stable adsorbed species at 100 K. The adsorbed CO_2 can only be observed on Au(111) surface at 100 K when an equilibrium between adsorption and desorption is established by bathing the sample in an atmosphere of 5×10^{-8} mbar CO_2. Correspondingly, an IRA spectrum taken after exposure of Au(111) to CO_2 followed by pumping gives a flat baseline in the ν_3 region (Figure 8b, middle). In CO_2 atmosphere (top spectrum in Figure 8b), however, surprisingly the spectrum contains in addition to a "regular" CO_2 species with a ν_3 (2341 cm^{-1}) close to that of gas-phase CO_2, the two side-bands that are also present on Au(111)-PDI_L, at similar frequencies. (Note that the side bands do not correspond to the rotational *P*- and *R*-branches of the vibrational spectrum of gas-phase CO_2). Two important conclusions can be drawn from this observation: First, the presence of CO_2 species giving rise to these particular vibrations is not directly related to adsorbed PDI on Au(111), making its assignment to 2D CO_2 overlayers most plausible. Second, the 2D overlayer is stabilized by the presence of PDI, which concurs with the STM observation that the seeding effect of $CO_2^{\delta-}$ stabilizes the formation of extended 2D clusters and monolayer films (Figure 3 and 4).

Finally, we comment on the large positive and negative shifts of the two bands related to 2D CO_2 from the gas-phase ν_3 vibrational frequency. Vibrations at 2390 and 2280 cm^{-1} are not unusual for physisorbed CO_2. The former one in combination with a vibrational mode at $\sim$2340 cm^{-1} have been assigned to the longitudinal optical (LO) and transverse optical (TO) phonon modes of crystalline and amorphous CO_2 ices.[62] The low frequency vibration at 2280 cm^{-1} is in the range of the ν_3 mode of $^{13}CO_2$. For the present study, both of these possibilities can be discarded because (1) the LO-TO splitting can only be observed in 3D CO_2 ices, and (2) the intensity of the 2280 cm^{-1} mode is much larger than expected for the 1% natural abundance of ^{13}C. Because the two bands at 2390 and 2280 cm^{-1} appear to be coupled an interpretation in terms of a splitting of the ν_3 mode into an *in-phase* and *out-of-phase* excitation of two translationally inequivalent CO_2 molecules in the unit-cell (Davydov splitting) of an ordered CO_2 overlayer structure seems more plausible. In fact, 2D overlayers of CO_2 readily form at low temperature on insulator surfaces such as MgO(001), KCl(001), CsF(100) or NaCl(001), and their structure has been investigated in detail by polarized IR, low energy electron diffraction, and helium atom scattering experiments.[62−67] Davydov splittings for these systems are in the range of 10−30 cm^{-1}, much smaller than observed in the present case and consistent with the known gas phase splittings.[43,68] The Davydov splitting on a metal surface can be larger than expected from the gas phase transition dipole moment of 0.32 D for CO_2, as well as the observed splittings on insulator surfaces, due to the enhancement of the transition dipole as well as resonant dipole−dipole interactions including the image dipoles at metal surfaces. For molecules such as CO the Davydov splitting can exceed 100 cm^{-1}, which is larger than predicted theoretically based on simple models of screening at metal surfaces.[69,70] The splitting of the ν_3 mode of CO_2 on Au(111) surface is expected for two molecules per surface unit cell in the rhombic structure, and its magnitude relative to the gas phase and insulator surfaces is consistent with those for other molecular overlayers on metals.

DISCUSSION

The CO_2 molecule/Au-PDI chain/Au surface system reveals a fascinating example of adsorption-induced

collective surface behavior of metal–organic surface polymer in response to chemical stimulation by CO_2 molecules. Decorating metal surfaces with submonolayer thick metal–organic films offers a novel strategy for activating catalytic reactions. The Au surfaces and Au-organic polymer with no known catalytic activity with respect to CO_2 reduction, becomes highly active when combined under UHV conditions. Organic molecules with strongly electron donating or withdrawing functional groups can form 1D or 2D metal–organic chains and webs where the metal adatoms acquire exceptional catalytic properties.[71] Because of charge transfer and reduced coordination number, metal atoms within such constructs can interact with target molecules in novel ways akin to inorganic homogeneous catalysts, offering metal atom coordination sites to reactants that are not available on low-index metal surfaces. Moreover, organic molecule ligands can be functionalized to amplify the charge transfer interactions to stabilize the $CO_2^{\delta-}$ species and other products in a manner that has been exploited by plants in photosynthetic carbon fixation as well as model systems that mimic the metal–organic reactive sites.[72−74] The catalytic properties of such metal–organic constructs will be revealed by further exploration of new substrates and reactants.

The ability to image structural response with molecular resolution and spectroscopically characterize the charge state of the surface species, their interactions, and chemically stimulated responses offers an unprecedented model for catalytic processes relevant to CO_2 capture and reduction. On the basis of molecule resolved STM imaging and charge transfer sensitive spectroscopic measurements of CO_2 chemisorption and physisorption on Au-PDI chain decorated Au surfaces, the following picture emerges. PDI molecules with isocyanide groups having major carbene and minor zwitterionic[75] character form covalent bonds with Au adatoms with accompanying charge transfer to the substrate. This charge transfer is enabled by the electron rich character of PDI molecules and expressed in a large reduction of the surface work function upon formation of Au-PDI chains;[38] it contributes to the strength of dipoles giving rise to a repulsive dipole–dipole interaction, which spreads the chains apart into parallel, equally spaced arrays. Upon exposure to CO_2, the charge donated by PDI molecules is available and, with the work function reduced, can be transferred to CO_2 molecules interacting with the Au adatom sites. The charge redistribution and chemical interactions enabled by $CO_2^{\delta-}$ chemisorption turn the chain–chain interaction from repulsive to attractive. The spectroscopic evidence from IRAS is consistent with the transfer of substantial part of electron charge to CO_2. The facile nanometer scale translational motion of Au-PDI chains at 77 K enables the surface to optimize interactions with CO_2 molecules. This motional freedom of the 1D MOC chains is the key feature of 1D surfaces[76] that enables the collective response, which would be more constrained in 2D or 3D polymers.

With the Au-PDI chains frozen at 4.5 K, the STM measurements show that the chemisorbed $CO_2^{\delta-}$ species at the adatom sites are stabilized by the physisorption and clustering of highly polarizable CO_2 molecules into 2D clusters. The cooperative interactions among CO_2 molecules persist to higher temperatures, where they are reflected in the Davydov splitting in the IRA spectra and the multicomponent evolution of the TPD spectra. Such cooperative anion-neutral interactions have been studied in gas phase for CO_2 anion clusters, $CO_2^{\delta-}\cdot(CO_2)_n$, by mass, photoelectron, and electron scattering spectroscopic methods.[77−85] Moreover, gas phase ion clusters including metal (M) atoms have also emerged as useful platforms for studying the interplay of the chemically active M-$CO_2^{\delta-}$ species, and their solvation shells of physically interacting CO_2 molecules.[61,84,86] For the surface supported Au-PDI chains the solvation of anionic species occurs under the influence of the metal substrate, which favors 2D cluster growth. The $CO_2^{\delta-}$ species seeds and anchors the growth of 2D crystalline structures into highly ordered overlayers, which adopt a rhombic phase due to interactions with the substrate. The entire process is reversible by ramping the temperature to activate desorption of physisorbed and chemisorbed CO_2 molecules.

CONCLUSIONS

Using surface science imaging and spectroscopic tools we have investigated the chemisorption of CO_2 molecules on Au-PDI decorated Au single crystal surfaces, and how such CO_2–Au adatom interactions promote the nucleation and growth of physisorbed clusters from dimers to full monolayers. The LT-STM images identify distinct chemisorption sites where $CO_2^{\delta-}$ forms by charge transfer from the substrate. The XP and IRA spectra are consistent with the transfer of considerable electron charge to two CO_2 molecules per Au adatom. The promoted nucleation enables STM visualization of the progressive physisorbed layer growth from dimers to 1D chains, 2D islands, eventually terminating in 2D monolayer domains, which are bounded by Au-PDI chains. The propensity of chemisorbed $CO_2^{\delta-}$ species to condense clusters over nanometer length scales suggests that the chemistry at such sites can be significantly modified by secondary interactions, which are triggered by the primary chemisorption process. The control of secondary interactions, as occurs in carbon fixation by plants,[72] may hold the clue to realizing efficient, low energy pathways for CO_2 capture and conversion into useful chemical products. Our work thus provides an experimental avenue for exploring the microscopic insights in the

CO_2 capture and reduction, as well as for exploring the nature of weak intermolecular forces in physical phenomena such as molecular condensation and ion solvation.

METHODS

Upon dosing PDI molecules at room temperature, 1D [-Au-PDI-]$_n$ chains self-assemble into parallel arrays on clean Au(100) and Au(111) surfaces. The PDI molecule dose determines the Au-PDI chain coverage, and thus the density of the chains on the surfaces. For the STM experiments, CO_2 molecules are dosed *in situ* at 20 K onto the MOC covered surfaces. STM constant current topographic images are taken at 4.5 K with a current of 0.1 nA and bias voltage of 0.1 V. The XPS, IRAS and TPD measurements are performed in a separate apparatus where the low-coverage [Au(111)-PDI$_L$] and high-coverage [Au(111)-PDI$_H$] samples are prepared. TPD scans and XP spectra (O 1*s* and C 1*s* region) are taken after dosing CO_2 (saturation at 100 K) to Au(111) and PDI-Au(111). The Au(111) work function changes induced by PDI desorption are obtained from determining the low kinetic energy cutoff of the corresponding XP spectra. For the IRAS measurement, room temperature spectra of clean and PDI dosed Au(111) are obtained first. Then the sample is cooled to 213 K to record a new background spectrum. CO_2 molecules are introduced into the UHV chamber through a leak valve at a sample temperature of 213 K and subsequent spectra are recorded while cooling the sample with the CO_2 background pressure of 5×10^{-8} mbar. After reaching the lowest temperature, CO_2 is evacuated from the chamber and a spectrum is recorded. This spectrum then serves as reference for the later ones recorded during the warming phase. First-principles calculations at DFT-D level are described in the Supporting Information.

Conflict of Interest: The authors declare no competing financial interest.

Acknowledgment. The authors acknowledge DOE-BES Division of Chemical Sciences, Geosciences, and Biosciences Grant No. DE-FG02-09ER16056 and NSFC 11322434, 21421063. Some calculations were performed at the Environmental Molecular Sciences Laboratory at the PNNL, a user facility sponsored by the DOE Office of Biological and Environmental Research. H.P. acknowledges support from the Alexander von Humboldt Research Award and the Chinese Academy of Sciences President's International Fellowship, and F.C. acknowledges the Alexander-von-Humboldt foundation for a Georg Forster fellowship.

Supporting Information Available: The Supporting Information is available free of charge on the ACS Publications website at DOI: 10.1021/acsnano.5b05222.

First-principles calculations on CO_2 physisorbed monolayer structures and CO_2 chemisorption structures at PDI chains. (PDF)

REFERENCES AND NOTES

1. Freund, H. J.; Roberts, M. W. Surface Chemistry of Carbon Dioxide. *Surf. Sci. Rep.* **1996**, *25*, 225–273.
2. Burghaus, U. Surface Science Perspective of Carbon Dioxide Chemistry-Adsorption Kinetics and Dynamics of CO_2 on Selected Model Surfaces. *Catal. Today* **2009**, *148*, 212–220.
3. Burghaus, U. Surface Chemistry of CO_2 – Adsorption of Carbon Dioxide on Clean Surfaces at Ultrahigh Vacuum. *Prog. Surf. Sci.* **2014**, *89*, 161–217.
4. Goeppert, A.; Czaun, M.; Jones, J.-P.; Surya Prakash, G. K.; Olah, G. A. Recycling of Carbon Dioxide to Methanol and Derived Products - Closing the Loop. *Chem. Soc. Rev.* **2014**, *43*, 7995–8048.
5. Bartos, B.; Freund, H. J.; Kuhlenbeck, H.; Neumann, M.; Lindner, H.; Müller, K. Adsorption and reaction of CO_2 and CO_2/O Co-adsorption on Ni(110): Angle Resolved Photoemission (ARUPS) and Electron Energy Loss (HREELS) Studies. *Surf. Sci.* **1987**, *179*, 59–89.
6. Freund, H. J.; Behner, H.; Bartos, B.; Wedler, G.; Kuhlenbeck, H.; Neumann, M. CO_2 Adsorption and Reaction on Fe(111): An Angle Resolved Photoemission (ARUPS) Study. *Surf. Sci.* **1987**, *180*, 550–564.
7. Paul, J. Vibrational Spectra of CO and CO_2 Adsorbed on Potassium Modified Fe(100). *Surf. Sci.* **1989**, *224*, 348–358.
8. Wambach, J.; Odörfer, G.; Freund, H. J.; Kuhlenbeck, H.; Neumann, M. Influence of Alkali Co-Adsorption on the Adsorption and Reaction of CO_2 on Pd(111). *Surf. Sci.* **1989**, *209*, 159–172.
9. Wohlrab, S.; Ehrlich, D.; Wambach, J.; Kuhlenbeck, H.; Freund, H. J. Promoter Action of Alkali in the Activation of CO_2 on Pd(111): A HREELS Case Study. *Surf. Sci.* **1989**, *220*, 243–252.
10. Maynard, K. J.; Moskovits, M. An Electron Energy Loss Study of Carbon Dioxide Adsorption on Alkali Metal Predosed Silver Surfaces. *Surf. Sci.* **1990**, *225*, 40–46.
11. Solymosi, F. The Bonding, Structure and Reactions of CO_2 Adsorbed on Clean and Promoted Metal Surfaces. *J. Mol. Catal.* **1991**, *65*, 337–358.
12. Davies, P. R.; Roberts, M. W. Activation of Carbon Dioxide by Ammonia at Cu(100) and Zn(0001) Surface Leading to the Formation of A Surface Carbamate. *J. Chem. Soc., Faraday Trans.* **1992**, *88*, 361–368.
13. Okawa, Y.; Tanaka, K. STM Investigation of the Reaction of Ag-O Added Rows with CO_2 on a Ag(110) Surface. *Surf. Sci.* **1995**, *344*, L1207–L1212.
14. Hadenfeldt, S.; Benndorf, C.; Stricker, A.; Towe, M. Adsorption of CO_2 on K-Promoted Cu(111) Surfaces. *Surf. Sci.* **1996**, *352*, 295–299.
15. Ricart, J. M.; Habas, M. P.; Clotet, A.; Curulla, D.; Illas, F. Theoretical Study of CO_2 Activation on Pt(111) Induced by Coadsorbed K Atoms. *Surf. Sci.* **2000**, *460*, 170–181.
16. Davies, P. R.; Keel, J. M. The Reaction of Carbon Dioxide with Amines at a Cu(211) Surface. *Surf. Sci.* **2000**, *469*, 204–213.
17. Guo, X. C.; Madix, R. J. CO_2+O on Ag(110): Stoichiometry of Carbonate Formation, Reactivity of Carbonate with CO, and Reconstruction-Stabilized Chemisorption of CO_2. *J. Phys. Chem. B* **2001**, *105*, 3878–3885.
18. Ojifinni, R. A.; Gong, J. L.; Froemming, N. S.; Flaherty, D. W.; Pan, M.; Henkelman, G.; Mullins, C. B. Carbonate Formation and Decomposition on Atomic Oxygen Precovered Au(111). *J. Am. Chem. Soc.* **2008**, *130*, 11250–11251.
19. Calaza, F.; Stiehler, C.; Fujimori, Y.; Sterrer, M.; Beeg, S.; Ruiz-Oses, M.; Nilius, N.; Heyde, M.; Parviainen, T.; Honkala, K.; Häkkinen, H.; Freund, H.-J. Carbon Dioxide Activation and Reaction Induced by Electron Transfer at an Oxide–Metal Interface. *Angew. Chem., Int. Ed.* **2015**, *54*, 12484–12487.
20. Copperthwaite, R. G.; Davies, P. R.; Morris, M. A.; Roberts, M. W.; Ryder, R. A. The Reactive Chemisorption of Carbon Dioxide at Magnesium and Copper Surfaces at Low Temperature. *Catal. Lett.* **1988**, *1*, 11–19.
21. Asscher, M.; Kao, C. T.; Somorjai, G. A. High-Resolution Electron Energy Loss Spectroscopic Study of Carbon Dioxide Adsorbed on Rhenium(0001). *J. Phys. Chem.* **1988**, *92*, 2711–2714.
22. Carley, A. F.; Davies, P. R.; Roberts, M. W. Activation of Carbon Dioxide Leading to a Chemisorbed Carbamate Species at a Cu(100) Surface. *J. Chem. Soc., Chem. Commun.* **1989**, 677–679.
23. Nakamura, J.; A, R. J.; Campbell, C. T. Does CO_2 Dissociatevley Adsorb on Cu Surfaces? *J. Phys.: Condens. Matter* **1989**, *1*, SB149–SB160.

24. Carley, A. F.; Davies, P. R.; Robers, M. W. Activation of Carbon Dioxide Leading to A Chemisorbed Carbamate Species at A Cu(100) Surface. *J. Chem. Soc., Chem. Commun.* **1989**, 677–679.
25. Browne, V. M.; Carley, A. F.; Copperthwaite, R. G.; Davies, P. R.; Moser, E. M.; Roberts, M. W. Activation of Carbon Dioxide at Bismuth, Gold and Copper Surfaces. *Appl. Surf. Sci.* **1991**, *47*, 375–379.
26. Ernst, K. H.; Schlatterbeck, D.; Christmann, K. Adsorption of Carbon Dioxide on Cu(110) and on Hydrogen and Oxygen Covered Cu(110) Surfaces. *Phys. Chem. Chem. Phys.* **1999**, *1*, 4105–4112.
27. Guo, X.-C.; Madix, R. J. CO_2 + O on Ag(110): Stoichiometry of Carbonate Formation, Reactivity of Carbonate with CO, and Reconstruction-Stabilized Chemisorption of CO_2. *J. Phys. Chem. B* **2001**, *105*, 3878–3885.
28. Guo, X. C.; Madix, R. J. Carbonate on Ag(110): A Complex System Clarified by STM. *Surf. Sci.* **2001**, *489*, 37–44.
29. Schumacher, N.; Andersson, K.; Grabow, L. C.; Mavrikakis, M.; Nerlov, J.; Chorkendorff, I. Interaction of Carbon Dioxide with Cu Overlayers on Pt(111). *Surf. Sci.* **2008**, *602*, 702–711.
30. Li, S. F.; Guo, Z. X. CO_2 Activation and Total Reduction on Titanium(0001) Surface. *J. Phys. Chem. C* **2010**, *114*, 11456–11459.
31. Posada-Perez, S.; Vines, F.; Ramirez, P. J.; Vidal, A. B.; Rodriguez, J. A.; Illas, F. The Bending Machine: CO_2 Activation and Hydrogenation on δ-MoC(001) and β-Mo_2C(001). *Phys. Chem. Chem. Phys.* **2014**, *16*, 14912–14921.
32. Dri, C.; Peronio, A.; Vesselli, E.; Africh, C.; Rizzi, M.; Baldereschi, A.; Peressi, M.; Comelli, G. Imaging and Characterization of Activated CO_2 Species on Ni(110). *Phys. Rev. B: Condens. Matter Mater. Phys.* **2010**, *82*, 165403.
33. Aoki, K.; Yamawaki, H.; Sakashita, M.; Gotoh, Y.; Takemura, K. Crystal Structure of the High-Pressure Phase of Solid CO_2. *Science* **1994**, *263*, 356–358.
34. Li, J.; Sode, O.; Voth, G. A.; Hirata, S. A Solid−Solid Phase Transition in Carbon Dioxide at High Pressures and Intermediate Temperatures. *Nat. Commun.* **2013**, *4*, 2647.
35. Boscoboinik, J. A.; Calaza, F. C.; Habeeb, Z.; Bennett, D. W.; Stacchiola, D. J.; Purino, M. A.; Tysoe, W. T. One-Dimensional Supramolecular Surface Structures: 1,4-Diisocyanobenzene on Au(111) Surfaces. *Phys. Chem. Chem. Phys.* **2010**, *12*, 11624–11629.
36. Boscoboinik, J.; Kestell, J.; Garvey, M.; Weinert, M.; Tysoe, W. T. Creation of Low-Coordination Gold Sites on Au(111) Surface by 1,4-Phenylene Diisocyanide Adsorption. *Top. Catal.* **2011**, *54*, 20–25.
37. Kestell, J.; Abuflaha, R.; Boscoboinik, J. A.; Bai, Y.; Bennett, D. W.; Tysoe, W. T. Linking Gold Nanopartilces with Conductive 1, 4-Phenylene Diiscocyanide-Gold Oligomers. *Chem. Commun.* **2013**, *49*, 1422–1424.
38. Zhou, J.; Acharya, D.; Camillone, N.; Sutter, P.; White, M. G. Adsorption Structures and Electronic Properties of 1,4-Phenylene Diisocyanide on the Au(111) Surface. *J. Phys. Chem. C* **2011**, *115*, 21151–21160.
39. Feng, M.; Sun, H.; Zhao, J.; Petek, H. Self-Catalyzed Carbon Dioxide Adsorption by Metal−Organic Chains on Gold Surfaces. *ACS Nano* **2014**, *8*, 8644–8652.
40. Edmonds, T.; Pitkethly, R. C. The Adsorption of Carbon Monoxide and Carbon Dioxide at the (111) Surface of Nickel Observed by LEED. *Surf. Sci.* **1969**, *15*, 137–163.
41. Krause, J.; Borgmann, D.; Wedler, G. Photoelectron Spectroscopic Study of the Adsorption of Carbon Dioxide on Cu(110) and Cu(110)/K - As Compared with the Systems Fe(110)/CO_2 and Fe(110)/K+CO_2. *Surf. Sci.* **1996**, *347*, 1–10.
42. Kao, C.-L.; Carlsson, A.; Madix, R. J. The Adsorption Dynamics of Molecular Carbon Dioxide on Pt(111) and Pd(111). *Surf. Sci.* **2002**, *497*, 356–372.
43. Weida, M. J.; Sperhac, J. M.; Nesbitt, D. J. High-resolution infrared diode laser spectroscopy of $(CO_2)_3$: Vibrationally Averaged Structures, Resonant Dipole Vibrational Shifts, and Tests of CO_2--CO_2 Pair Potentials. *J. Chem. Phys.* **1995**, *103*, 7685–7699.
44. Saeki, M.; Tsukuda, T.; Nagata, T. *Ab initio* Study of $(CO_2)_n^-$: Structures and Stabilities of Isomers. *Chem. Phys. Lett.* **2001**, *340*, 376–384.
45. Torrisi, A.; Mellot-Draznieks, C.; Bell, R. G. Impact of Ligands on CO_2 Adsorption in Metal-Organic Frameworks: First Principles Study of the Interaction of CO_2 with Functionalized Benzenes. I. Inductive Effects on the Aromatic Ring. *J. Chem. Phys.* **2009**, *130*, 194703–13.
46. Grimme, S. Semiempirical GGA-Type Density Functional Constructed with a Long-Range Dispersion Correction. *J. Comput. Chem.* **2006**, *27*, 1787–1799.
47. Pranger, L.; Tannenbaum, R. Self-Assembly of 1,4-Phenylene Diisocyanide and Terephthalic Acid on Ni, Cu and Pt. *J. Colloid Interface Sci.* **2005**, *292*, 71–78.
48. Illing, G.; Heskett, D.; Plummer, E. W.; Freund, H. J.; Somers, J.; Lindner, T.; Bradshaw, A. M.; Buskotte, U.; Neumann, M.; Starke, U.; Heinz, K.; De Andres, P. L.; Saldin, D.; Pendry, J. B. Adsorption and Reaction of CO_2 on Ni{110}: X-Ray Photoemission, Near-Edge X-ray Absorption Fine-Structure and Diffuse LEED Studies. *Surf. Sci.* **1988**, *206*, 1–19.
49. Carley, A. F.; Roberts, M. W.; Strutt, A. J. Activation of Carbon Monoxide and Carbon Dioxide at Cesium-Promoted Cu(110) and Cu(110)-O Surfaces. *J. Phys. Chem.* **1994**, *98*, 9175–9181.
50. Ding, X.; De Rogatis, L.; Vesselli, E.; Baraldi, A.; Comelli, G.; Rosei, R.; Savio, L.; Vattuone, L.; Rocca, M.; Fornasiero, P.; Ancilotto, F.; Baldereschi, A.; Peressi, M. Interaction of Carbon Dioxide with Ni(110): A Combined Experiemntal and Theoretical Study. *Phys. Rev. B: Condens. Matter Mater. Phys.* **2007**, *76*, 195425.
51. Deng, X. Y.; Verdaguer, A.; Herranz, T.; Weis, C.; Bluhm, H.; Salmeron, M. Surface Chemistry of Cu in the Presence of CO_2 and H_2O. *Langmuir* **2008**, *24*, 9474–9478.
52. Henderson, J. I.; Feng, S.; Bein, T.; Kubiak, C. P. Adsorption of Diisocyanides on Gold. *Langmuir* **2000**, *16*, 6183–6187.
53. Kim, H. S.; Lee, S. J.; Kim, N. H.; Yoon, J. K.; Park, H. K.; Kim, K. C. Adsorption Characteristics of 1,4-Phenylene Diisocyanide on Gold Nanoparticles: Infrared and Raman Spectroscopy Study. *Langmuir* **2003**, *19*, 6701–6710.
54. Murphy, K. L.; Tysoe, W. T.; Bennett, D. W. A Comparative Investigation of Aryl Isocyanides Chemisorbed to Palladium and Gold: An ATR-IR Spectroscopic Study. *Langmuir* **2004**, *20*, 1732–1738.
55. Hoffmann, F. M.; Weisel, M. D.; Paul, J. The Activation of CO_2 by Potassium-Promoted Ru(001) I. FT-IRAS and TDMS Study of Oxalate and Carbonate Intermediates. *Surf. Sci.* **1994**, *316*, 277–293.
56. Farkas, A. P.; Solymosi, F. Activation and Reactions of CO_2 on a K-Promoted Au(111) Surface. *J. Phys. Chem. C* **2009**, *113*, 19930–19936.
57. Hartman, K. O.; Hisatsune, I. C. Infrared Spectrum of Carbon Dioxide Anion Radical. *J. Chem. Phys.* **1966**, *44*, 1913–1918.
58. Jacox, M. E.; Thompson, W. E. The Vibrational Spectra of Molecular Ions Isolated in Solid Neon. I. CO_2^+ and CO_2^-. *J. Chem. Phys.* **1989**, *91*, 1410–1416.
59. Thompson, W. E.; Jacox, M. E. The Vibrational Spectra of CO_2^+,$(CO_2)_2^+$,CO_2^-, and $(CO_2)_2^-$ Trapped in Solid Neon. *J. Chem. Phys.* **1999**, *111*, 4487–4496.
60. Freund, H. J.; Messmer, R. P. On the Bonding and Reactivity of CO_2 on Metal Surfaces. *Surf. Sci.* **1986**, *172*, 1–30.
61. Knurr, B. J.; Weber, J. M. Solvent-Driven Reductive Activation of Carbon Dioxide by Gold Anions. *J. Am. Chem. Soc.* **2012**, *134*, 18804–18808.
62. Baratta, G. A.; Palumbo, M. E. Infrared Optical Constants of CO and CO_2 Thin Icy Films. *J. Opt. Soc. Am. A* **1998**, *15*, 3076–3085.
63. Heidberg, J.; Meine, D.; Redlich, B. CO_2 Adsorption on the MgO(100) Single Crystal Surface Detected by Polarization FTIR Spectroscopy and SPA-LEED. *J. Electron Spectrosc. Relat. Phenom.* **1993**, *64−65*, 599–608.
64. Heidberg, J.; Kampshoff, E.; Kühnemuth, R.; Schönekäs, O.; Lange, G.; Schmicker, D.; Toennies, J. P.; Vollmer, R.; Weiss, H. 'Internal' and 'External' Vibrational Modes of CO_2/NaCl(001) Studied by Fourier-Transform Infrared Spectroscopy and Helium Atom Scattering. *J. Electron Spectrosc. Relat. Phenom.* **1993**, *64−65*, 341–350.
65. Heidberg, J.; Redlich, B. The Adsorption of CO_2 and N_2O on the MgO(001) Single Crystal Surface: A Comparative PIRSS and LEED Study. *Surf. Sci.* **1996**, *368*, 140–146.

66. Heidberg, J.; Henseler, H. The Physisorption of CO_2 and the Stepwise Chemisorption of SO_2 on the CsF(100) Single Crystal Surface. *Surf. Sci.* **1999**, *427−428*, 439–445.
67. Traeger, F.; Hadnadjev, M.; Vogt, J.; Weiss, H. Structure of CO_2 Adsorbed on the KCl(100) Surface. *J. Phys. Chem. A* **2011**, *115*, 6986–6996.
68. Oliaee, J. N.; Dehghany, M.; Moazzen-Ahmadi, N.; McKellar, A. R. W. Spectroscopic Identification of Carbon Dioxide Clusters: $(CO_2)_6$ to $(CO_2)_{13}$. *Phys. Chem. Chem. Phys.* **2011**, *13*, 1297–1300.
69. Mahan, G. D.; Lucas, A. A. Collective Vibrational Modes of Adsorbed CO. *J. Chem. Phys.* **1978**, *68*, 1344–1348.
70. Voigtländer, B.; Bruchmann, D.; Lehwald, S.; Ibach, H. Structure and Adsorbate-Adsorbate Interactions of the Compressed Ni(110)-(2 × 1)CO Structure. *Surf. Sci.* **1990**, *225*, 151–161.
71. Grumelli, D.; Wurster, B.; Stepanow, S.; Kern, K. Bio-Inspired Nanocatalysts for the Oxygen Reduction Reaction. *Nat. Commun.* **2013**, *4* (2904), 1–6.
72. Stec, B. Structural Mechanism of RuBisCO Activiation by Carbamylation of the Active Site Lysine. *Proc. Natl. Acad. Sci. U. S. A.* **2012**, *109*, 18785.
73. McDonald, T. M.; Mason, J. A.; Kong, X.; Bloch, E. D.; Gygi, D.; Dani, A.; Crocella, V.; Giordanino, F.; Odoh, S. O.; Drisdell, W. S.; Vlaisavljevich, B.; Dzubak, A. L.; Poloni, R.; Schnell, S. K.; Planas, N.; Lee, K.; Pascal, T.; Wan, L. F.; Prendergast, D.; Neaton, J. B.; Smit, B.; Kortright, J. B.; Gagliardi, L.; Bordiga, S.; Reimer, J. A.; Long, J. R. Cooperative Insertion of CO_2 in Diamine-Appended Metal-Organic Frameworks. *Nature* **2015**, *519*, 303–308.
74. Cooper, A. I. Materials Chemistry: Cooperative Carbon Capture. *Nature* **2015**, *519*, 294–295.
75. Ramozzi, R.; Cheron, N.; Braida, B.; Hiberty, P. C.; Fleurat-Lessard, P. A Valence Bond view of Isocyanides' Electronic Structure. *New J. Chem.* **2012**, *36*, 1137–1140.
76. Feng, M.; Lin, C.; Zhao, J.; Petek, H. Orthogonal Intermolecular Interactions of CO Molecules on a One-Dimensional Substrate. *Annu. Rev. Phys. Chem.* **2012**, *63*, 201–224.
77. Klots, C. E.; Compton, R. N. Electron Attachment to Van der Waals Polymers of Carbon Dioxide and Nitrous Oxide. *J. Chem. Phys.* **1978**, *69*, 1636–1643.
78. Bowen, K. H.; Liesegang, G. W.; Sanders, B. S.; Herschbach, D. R. Electron Attachment to Molecular Clusters by Collisional Charge Transfer. *J. Phys. Chem.* **1983**, *87*, 557–565.
79. Stamatovic, A.; Leiter, K.; Ritter, W.; Stephan, K.; Märk, T. D. Electron Attachment to Carbon Dioxide Clusters at Very Low Electron Energies. *J. Chem. Phys.* **1985**, *83*, 2942–2946.
80. Fleischman, S. H.; Jordan, K. D. Theoretical Study of the Structures and Stabilities of the Carbon Dioxide Dimer ($(CO_2)_2^-$) Ions. *J. Phys. Chem.* **1987**, *91*, 1300–1302.
81. DeLuca, M. J.; Niu, B.; Johnson, M. A. Photoelectron Spectroscopy of $(CO_2)_n^-$ Clusters with $2 \leq n \leq 13$: Cluster Size Dependence of the Core Molecular Ion. *J. Chem. Phys.* **1988**, *88*, 5857–5863.
82. Gutsev, G. L.; Bartlett, R. J.; Compton, R. N. Electron Affinities of CO_2, OCS, and CS_2. *J. Chem. Phys.* **1998**, *108*, 6756–6762.
83. Huels, M. A.; Bass, A. D.; Ayotte, P.; Sanche, L. Absolute Cross Sections for Anion Production by Low Energy Electron Impact on Physisorbed CO_2. *Chem. Phys. Lett.* **1995**, *245*, 387–392.
84. Shin, J. W.; Hammer, N. I.; Johnson, M. A.; Schneider, H.; Glöβ, A.; Weber, J. M. An Infrared Investigation of the $(CO_2)_n^-$ Clusters: Core Ion Switching from Both the Ion and Solvent Perspectives. *J. Phys. Chem. A* **2005**, *109*, 3146–3152.
85. Michaud, M.; Hébert, E. M.; Cloutier, P.; Sanche, L. Electron Photoemission from Charged Films: Absolute Cross Section for Trapping 0−5eV Electrons in Condensed CO_2. *J. Chem. Phys.* **2007**, *126*, 024701.
86. Weber, J. M. The Interaction of Negative Charge with Carbon Dioxide − Insight into Solvation, Speciation and Reductive Activation from Cluster Studies. *Int. Rev. Phys. Chem.* **2014**, *33*, 489–519.